HHS Public Access

Author manuscript

J Colloid Interface Sci. Author manuscript; available in PMC 2020 October 01.

Published in final edited form as:

J Colloid Interface Sci. 2019 October 01; 553: 136–147. doi:10.1016/j.jcis.2019.06.016.

Flow regime transitions and effects on solute transport in surfactant-driven Marangoni flows

Steven V. Iasella[a], **Ningguan Sun**[a], **Xin Zhang**[a], **Timothy E. Corcoran**[b], **Stephen Garoff**[c],*, **Todd M. Przybycien**[a],[d],[1], **Robert D. Tilton**[a],[d],*

[a] Department of Chemical Engineering, Center for Complex Fluids Engineering, Carnegie Mellon University, Pittsburgh, PA 15213

[b] Pulmonary, Allergy, and Critical Care Division, Department of Medicine, University of Pittsburgh, Pittsburgh, PA 15260

[c] Department of Physics, Center for Complex Fluids Engineering, Carnegie Mellon University, Pittsburgh, PA 15213

[d] Department of Biomedical Engineering, Center for Complex Fluids Engineering, Carnegie Mellon University, Pittsburgh, PA 15213

Abstract

Hypothesis—Surfactant driven Marangoni flow on liquid films is predicted to depend on subphase depth and initial surface tension difference between the subphase and deposited surfactant solution drop. Changes in flow behavior will impact transport of soluble species entrained in the Marangoni flow along the surface. In extreme cases, the subphase film may rupture, limiting transport. Understanding this behavior is important for applications in drug delivery, coatings, and oil spill remediation.

Experiments—A trans-illumination optical technique measured the subphase height profiles and drop content transport after drop deposition when varying initial subphase depth, surfactant concentration, and subphase viscosity.

Findings—Three distinct flow regimes were identified depending on the subphase depth and surfactant concentration and mapped onto an operating diagram. These are characterized as a “central depression” bounded by an outwardly traveling ridge, an “annular depression” bounded by a central dome and the traveling ridge, and an “annular dewetting” when the subphase ruptures. Well above the critical micelle concentration, transitions between regimes occur at characteristic ratios of gravitational and initial surface tension gradient stresses; transitions shift when surfactant

*Corresponding Authors: sg2e@andrew.cmu.edu (P:412-268-6877), tilton@cmu.edu (P:412-268-1159), Carnegie Mellon University: 5000 Forbes Ave, Pittsburgh, PA 15213, University of Pittsburgh School of Medicine: 3550 Terrace St, Pittsburgh, PA 15213, Rensselaer Polytechnic Institute: 110 8th St, Troy NT 12180.

[1]Present Address: Department of Chemical and Biological Engineering, Rensselaer Polytechnic Institute, Troy, NY 12180

Declarations of Interest: None

dilution during spreading weakens the stress before the completion of the spreading event. Drop contents travel with the ridge, but dewetting hinders transport.

Graphical Abstract

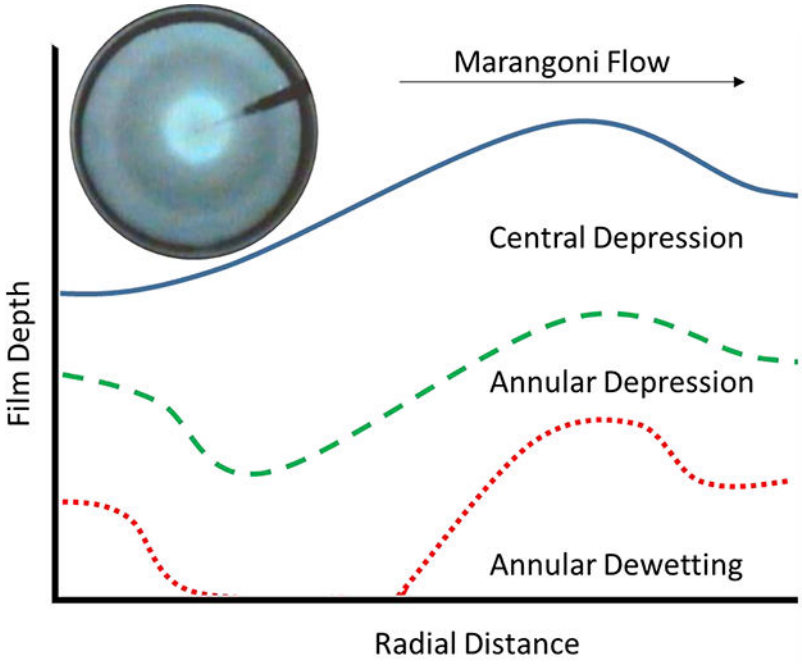

Keywords

Marangoni flow; spreading; surfactants; liquid films; dewetting

1. Introduction[1]

Surface tension driven stresses at interfaces (Marangoni stresses) have been of interest for the transport of materials in diverse applications, several of which involve transport on thin liquid films. One potential application is the post-deposition dispersal of inhaled aerosol medicines in the treatment of bacterial lung infections associated with diseases such as cystic fibrosis (CF)[1–8]. In CF patients, mucus plaques form in the lungs and limit the airborne dispersal of aerosolized antibiotics[9–11]. The use of Marangoni stresses may allow the drug to be transported along the airway surface liquid after deposition of the aerosol, leading to more uniform drug distribution and more effective treatments. Marangoni stresses are also of interest in the field of paints and coatings[12]. If surface active materials in these coatings are distributed non-uniformly, Marangoni stresses will deform the surface of the film. These films may then dry while deformed leading to unwanted unevenness in the coatings. These examples inherently involve thin films. A third example of the use of Marangoni flow is in oil spill remediation, where the flow occurs on a deep pool. One

[1]Abbreviations: cystic fibrosis (CF), surface tension (γ), radial coordinate (r), viscosity (μ), velocity (u), vertical coordinate (z), height of interface (H), initial height of interface (H0), gravity parameter (G), density (ρ), initial surface tension difference (S), gravitational acceleration (g), critical micelle concentration (CMC), sodium dodecyl sulfate (SDS)

method of oil spill remediation uses surfactants as “herders” to corral the oil spill into a smaller region where it can be contained and eliminated[13]. An understanding of Marangoni stresses and their impact on material transport, both of the contents of the surfactant source and of the underlying liquid itself, are needed in order to design formulations for these and other applications.

Depositing surfactants on a localized region of a liquid/vapor interface creates a surface tension gradient between that point and the clean surface away from the deposition region. The surface tension gradient causes Marangoni flow of the surfactant at the surface as well as the liquid below[2,3,14–19]. Flow in the liquid as well as transport of the surfactant must satisfy the tangential stress boundary condition at the surface where surfactant is present[17]:

$$\frac{d\gamma}{dr} = \mu \frac{du}{dz}\Big|_{Z=H} \quad (1)$$

where γ is surface tension, r is the radial coordinate, μ is viscosity of the liquid, u is the liquid velocity, z is the normal coordinate, and $z = H$ represents the surface of the subphase that has depth H. At any surface position outside the surfactant-containing region, the surface tension gradient does not exist, and a shear free boundary condition is imposed. The spatial transition in the boundary condition deforms the surface to create a ridge that moves away from the deposition site and a depression behind the ridge[4,15,16]. This feature moves across the surface as the surfactant is transported outward from the deposition region. The height of the “Marangoni ridge” is limited by gravity driven recirculation flow in the vicinity of the ridge[3]. Using the lubrication approximation, Gaver and Grotberg[3] prescribe a dimensionless gravitational parameter G which relates the surface tension flow driving the ridge outward and the gravity driven recirculation flow back toward the deposition point, for a disk of surfactant on a thin liquid film:

$$G = \frac{H_0{}^2 \rho g}{S} \quad (2)$$

where ρ is the density of the subphase, g is gravitational acceleration, H_0 is the initial height of the surface, and S is the difference between the surface tension of the clean subphase and the surface tension in the region containing the initial surfactant deposit. While similar to a Bond number which relates gravitational stress to the surface tension stress, this gravitational parameter relates the gravitational stress to the surface tension gradient (Marangoni) stress along a fluid surface. Gaver and Grotberg predict types of behavior with important qualitative differences that depend on the gravitational parameter value[3].

For the first of the behaviors, the outward Marangoni flow creates hydrostatic forces that cause a recirculation flow of liquid back towards the region where the surfactant was originally deposited (schematic in Figure 1A). The surface deformation can be described as an outward moving ridge surrounding a central depression. This recirculation flow is predicted to occur nearly simultaneously with the onset of flow for systems with G>1, and at

delayed times for systems with smaller G values, assuming a laterally unbounded subphase and an insoluble surfactant. Within this model, the depth of the depression of the interface behind the traveling Marangoni ridge is controlled by the recirculation flow and therefore is quantitatively dependent on the value of G.

Below a lower threshold value of $G = 0.5$, all flow in the system now moves outward for a significant period of time before recirculation flows start to occur (schematic shown in Figure 1B)[3] and the surface deformation can be described as an annular depression. The duration of this time period depends on the initial surface tension gradient, depth and viscosity of the subphase, and radius of the surfactant disc. The suppression of recirculation flow may produce a situation where if enough liquid leaves the surfactant deposition region before recirculation occurs, the liquid film may rupture and expose the solid substrate below the liquid layer. This dewetting behavior has been predicted and observed in several other theoretical and experimental studies of Marangoni spreading on thin films, and is often accompanied by a fingering instability near the edge of the dewet surface[14,15,19–25].

While these studies do much to elucidate the behavior of Marangoni spreading, most consider solvent-free “disks” of surfactant located on the surface rather than deposited surfactant solution drops. Karapetsas and coworkers have taken a modeling approach to understand how surfactant-containing drops spread along surfaces when the drop is immiscible with the subphase[26]. Larger subphase depths were predicted to produce larger velocities due to the greater distance between the liquid surface and the bottom solid substrate where the no slip boundary condition is imposed. Changing the initial surface tension difference (S) changed the shape of the spreading surfactant drop, with a larger surface tension difference leading to more highly deformed, thinned drops during spreading. In this model, surfactants were allowed to escape from the drop by mass transfer directly to the subphase/vapor interface. High rates of surfactant mass transfer from the drop to the surrounding surface allowed surfactant to migrate well beyond the drop edge, while small mass transfer rates led to the drop itself being more highly stretched and deformed across the surface.

The G parameter defined in Equation 2 highlights the importance of the initial surface tension difference between the surfactant deposit and the clean surface. This surface tension difference may not remain constant as the spreading proceeds. If the surfactant source is a drop of soluble surfactant solution, the drop may be depleted of surfactants by their diffusion into the subphase and by their adsorption to an expanding area of liquid/vapor interface. If during the spreading, sufficient surfactant is depleted from the drop such that the concentration falls below the critical micelle concentration (CMC), then the surface tension difference that drives the Marangoni flow must decrease as time proceeds.

Lee and Starov have shown that if a soluble surfactant solution well above its CMC is used to cause spreading, the effect of diluting the adsorbed surfactant surface concentration at the expanding surface can be mitigated[27]. As spreading dilutes the adsorbed surfactant layer, micelles in the bulk of the drop begin to disintegrate and release surfactant to adsorb to the interface and maintain constant surface concentration and surface tension. Once all of the micelles have disintegrated and the bulk of the drop is no longer above the CMC, the rate of

surfactant replenishment decreases and the local equilibrium between adsorbed surfactant and the bulk shifts to yield a higher local surface tension. Thus, the driving force for spreading decreases. We refer to this changing surface tension in the region of deposition during spreading as “depletion”. In the case of a soluble surfactant, the depletion point occurs whenever micelles in the surfactant drop all disintegrate and the surfactant equilibrium between the bulk and the surface begins to change. In the case of an insoluble surfactant the depletion point occurs whenever the surface concentration of the surfactant drops below a saturated monolayer in the region of deposition.

For an unbounded (infinite) surface, this depletion is an inherent property of the system. However, in bounded systems such as in a petri dish of finite radius, for a sufficiently large surfactant concentration, the depletion point may never be reached before the spreading front hits the dish boundary. Increasing the dish radius could allow the depletion point to be reached, making this an extrinsic property of the system. Furthermore, if the spreading event is expressed with the initial surface tension difference as the fundamental driver for the Marangoni spreading behavior, it must be borne in mind that this surface tension difference will be maintained for longer times and/or greater extents of spreading for solutions that are further above the CMC. Solutions just barely above the CMC will experience this surface tension depletion effect and the spreading driving force will begin to decrease immediately upon the start of spreading. The result is that systems with equal values of S may behave differently depending on the initial surfactant concentration or inventory in the drop.

The Marangoni spreading will also drive the transport of all components present in the surfactant laden drop. We have shown that surfactant moves out ahead of the spreading drop under many different spreading conditions[2,7,8,14]. However, these studies were all performed on relatively thick subphases (~1 cm) and had relatively high concentration detection thresholds for the dye used as a tracer in the drop. Considering one of the motivating applications of Marangoni spreading is to transport drug in the lung airways, where liquid layers can be as thin as 7 μm[11], film thickness may have drastic effects on spreading and transport behavior.

In this study, we develop a trans-illumination optical technique to measure and characterize Marangoni stress driven transport as a function of subphase thickness and surfactant concentration. This work expands on the prior theoretical[3,15,28] and experimental [29,30] studies in the literature to quantitatively test predicted flow regime transitions, identify factors that cause deviations from predicted trends, and establish the connection between the Marangoni flow regime and the transport of the bulk contents of a surfactant solution drop deposited on a miscible subphase. We make use of a Beer-Lambert law relationship for a chromophore incorporated in the subphase and drop phases to quantitatively track the surface height profile in one implementation of the technique and to quantitatively track drop contents transport using a dye incorporated into the applied drop in another implementation. We identify three distinct hydrodynamic regimes characterized by qualitative differences in the time-dependent subphase film height profile. By tracking height profiles, we confirm the ridge characteristics of two theoretically predicted flow regimes as well as the characteristics of a third regime where dewetting occurs. We generate a quantitative operating diagram for Marangoni spreading and show how these regimes

demonstrate distinct hydrodynamic behaviors. Regions of occurrence for these regimes on the operating diagram are compared against theoretical predictions based on the G parameter. The effect of surfactant depletion on the predictive value of the G parameter is determined. We further identify how the particular hydrodynamic regime can have a large effect on the transport of drop contents along the liquid subphase, especially concerning the amount of the drop contents that is transported along with the Marangoni ridge. We finish with a brief examination of spreading on complex subphases that indicates the influence of subphase viscosity on the hydrodynamic regime transitions. This work will facilitate the design of spreading solutions to achieve maximum material transport and to avoid undesirable dewetting behavior.

2. Materials and Methods

2.1 Materials

The surfactant sodium dodecylsulfate (>98.5%, Sigma Aldrich, Cat#L3771) (SDS) and the water-soluble dye erythrosine B (>80%, Sigma Aldrich, CAT#E8886) were purchased from Sigma-Aldrich and used as received. SDS purity was verified via the absence of a surface tension minimum at its CMC (Figure S5). All water was deionized and further purified to a resistivity of 18 MΩ·cm using a Milli-Q Academic unit (Millipore Corporation). Polyacrylamide (MW 5MDa-6MDa, Polysciences, Inc. Cat#02806), used to modify subphase viscosity, was solvated into the purified water over the course of several weeks on an orbital shaker in order to ensure complete dissolution. Pyrex glass petri dishes of radius 7 cm were used to hold the subphases for all experiments. All glassware was acid cleaned on the day of use with Nochromix® (Sigma Aldrich, CAT#328693) and sulfuric acid (>95%, Fischer scientific, CAT#A300–212) solution. Between experiments on the same day, the glassware was rinsed with ethanol (>99.5, Pharmco, CAT#111000200), acetone (>99.5%, Pharmco-Aaper, CAT#329000000), and purified water sequentially, and then dried using compressed nitrogen. All experiments were conducted at room temperature, 21±2°C.

2.2 Methods

2.2.1 Optical setup—An optical setup was developed (Figure 2) to map the height of the liquid layer during the spreading experiments. The experiment maps the optical density of a subphase that contains erythrosine B dye. The sample is illuminated from below with a diffuse white light source. The transmitted light intensity is measured as a function of position on the sample by imaging the surface with a color digital camera (640×480p×, 18p×/cm, 29 fps, Q-SEE CCD Camera, QPSCDNV) with a camera lens (1/3” 3.5–8mm f1.4 Varifocal, Fixed Iris CCTV Lens) and Elgato Video Capture system and software (Elgato). A 520 – 530 nm band-pass filter (Edmund Optics, CAT#65154) was placed in front of the camera lens so that the only light detected by the camera was close to the absorbance peak of the erythrosine B dye (530 nm, see supplemental information Figure S4). This permits the local subphase depth and local optical density to be related via the Beer-Lambert law. The linearity of calibration curves of optical density versus film thickness was verified for all film thicknesses used in the experiments (Supplemental Information Section S.1). When measuring the liquid film height profiles, both the subphase liquid and the surfactant solution drop have equal dye concentrations, so the measured subphase depth includes liquid

from the drop. Each frame is analyzed to yield a map of optical density that is converted to a map of subphase depth. In separate experiments that track the transport of drop contents, only the drop contains the dye. With no dye in the original subphase film, optical density maps track the local abundance of dye that originated from the drop.

2.2.2 Experimental Protocol—Two types of experiments were carried out, one where dye was included in the subphase and the drop (to determine the surface deformations and characterize the position and shape of the Marangoni ridge) and one where dye was included in only the drop (to determine the spreading of the drop contents). For both sets of experiments, SDS concentrations ranged from 0 –150 mM and subphase depths ranged from 0.3 – 2.4 mm. After accounting for the surface tension of the surfactant solutions, this corresponds to a range of $0.024 < G < 3.8$. A single 5 μL drop was gently deposited on the subphase by touching the drop formed at the tip of a pipette to the surface. Images were recorded and analyzed for the first 233 ms after spreading started to ensure that no data was contaminated by the reflection of the Marangoni ridge from the petri dish edge at later times. Surface tensions of the spreading solutions were measured with a Wilhelmy Pin Apparatus (Nima Technology Limited).

2.2.3 Data Analysis—The Beer-Lambert law relationship was constructed to determine the liquid height and amount of dye across the petri dish during the spreading event. Immediately before each experiment where dye was present in the subphase, images were recorded for three to five known liquid depths to act as calibration points for the Beer-lambert law relationship between recorded optical density and film thickness. An image was also recorded with no liquid in the petri dish to provide a map of incident intensity, I_o. Then, intensities, I, measured at each pixel in the calibrations and in the experiments were converted to optical density as is described in Supplemental Information section S.1 Equation S4. The erythrosine B extinction coefficient measured with the 530 – 540 nm bandpass filter was 50,800 cm^2/g. (The dye solution absorbance decreases by ~11% in the presence of the highest SDS concentration, 82.0 mM, due to solvatochromatic effects associated with dye partitioning into SDS micelles, but this has no significant effect on any conclusions drawn from these experiments.)

Details for taking into account the effect of surface reflections are discussed in the supplementary information (Section S.1). The Beer-Lambert law calibration between optical density and film height was calculated at each pixel location across the image in order to account for any spatial variation in lighting or pixel sensitivity that may have existed. The relationship specific to each pixel was used to calculate the corresponding film height at that location during the spreading experiment at every pixel for every frame. An azimuthal average of the height data was calculated using the center of the region of drop deposition as the origin, and azimuthally averaged heights were plotted as a function of radial position for every frame. The region of the image obscured by the pipette was excluded from this average. In order to analyze the solute-tracking experiments where dye is included only in the drop, a Beer-Lambert law relationship was constructed from the previously obtained optical density data by averaging the optical density across the dish at several different dye solution heights. This relationship, plotted in Figure S3 in the supplemental material, is then

used to calculate the azimuthally averaged column density of dye (number of dye molecules contained in a liquid column of unit area) in order to better understand the distribution of dye in and around the spreading drop.

3. Results

3.1 Method Development

Varying the SDS concentration in the drops varies the surface tension difference that drives Marangoni spreading. Since organic dyes are complex molecules that may interact with surfactants, the effect of erythrosine dye on the surface tension of SDS solutions was determined. The erythrosine concentration in the subphase and in the SDS solution drop was 0.05 g/L (0.06 mM) in experiments tracking subphase height profiles. In the drop contents tracking experiments with dye only in the drop, the erythrosine concentration in the drop was 50 g/L (60 mM). Figure S5 in the supplemental information shows the surface tension with respect to SDS concentration in aqueous solutions containing no dye or dye at 0.05 g/L or 50 g/L. The CMC for the dye/SDS solutions was shown to be lowered from 8 mM for the pure SDS to 6 and 4 mM for the 0.05 and 50 g/L solutions respectively. Most of the concentrations used in the spreading solution were above the CMC, producing the same initial surface tension of ~37mN/m. Depending on the SDS concentration, surfactant depletion could occur and begin to decrease the surface tension difference that drives the Marangoni spreading. 5 μL drops of solution were deposited to initiate the spreading event on a subphase surface with 170 cm^2 area. Since the saturated area/molecule of the monolayer is ~52.5 $Å^2$/molecule[31], drops with concentration below ~18 mM will experience depletion due to adsorption during the reported spreading events. Surfactant diffusion into the bulk subphase may allow even more concentrated solutions to experience depletion as well.

As shown in Figure S5 of the supplemental information, the dye concentrations used do have a noticeable effect on the relevant surface tension of the surfactant solutions, although erythrosine itself (in the absence of SDS) is only weakly surface active (Figure S.5). For this reason and because the two types of experiments use different dye concentrations, experiments tracking dye transport were only compared to experiments tracking surface deformation for conditions when the drop solution for both cases had the same initial surface tension. This was done so that the driving force for spreading, and thus the Marangoni flow behavior, would be the same between the two experiments. As a further precaution, comparisons were only made at large SDS concentrations where depletion would not occur. This ensured that the surface tension gradient driving force, and thus the Marangoni flow, would remain the same throughout the duration of both types of experiments. Finally, as will be discussed below, the three Marangoni flow regimes display quite different long-time behaviors. These were used as additional verification that drop content transport experiments were correctly matched to the appropriate hydrodynamic regime when examining the correlation between hydrodynamic regime and drop contents transport.

3.2 Subphase Height Profiles: Surface Distortion during Spreading

Three distinct surface shapes are observed during a spreading event, indicating that different hydrodynamic regimes occur depending on the height of the subphase and the concentration of the surfactant used. In Figure 3, examples of the height profiles for the three regimes (central depression, annular depression, and annular dewetting) are shown for the first 233 ms after drop deposition. This time was well before the spreading Marangoni ridge had reached the wall of the petri dish in all cases. The accuracy of the height analysis at each time point was checked by computing the total mass of the body of revolution formed by rotating the height curve around the *z*-axis. In all cases, the material balance closed to within 5%.

The first of the regimes is termed the central depression regime and is depicted in Figure 3A (for the case of 82.0 mM SDS and H_0 = 2.4 mm). In this regime, a depression forms in the center of the region of drop deposition which deepens and widens with time. The Marangoni ridge moves away from the region of deposition, at a speed to be discussed below. The shape of the surface height profile (a central depression inside the outwardly moving Marangoni ridge) is consistent with the theoretical prediction of Gaver and Grotberg whenever recirculation occurs[3].

The next regime is termed the annular depression regime and is depicted in Figure 3B (for the case of 82.0 mM SDS and H_0 = 1.2 mm). In this regime, the early stages resemble the central depression regime, but as time proceeds, a dome of liquid begins to form in the region of deposition. This dome is surrounded by a thinned annular film region, and beyond that is the Marangoni ridge. The annular depression deepens and moves outward as time proceeds. The thinned annular region does not dewet, but instead persists for up to 60 s before the liquid flows back to fill the depression. These surface height profiles are also consistent with the predictions of Gaver and Grotberg when recirculation does not occur (i.e. central dome, annular thinned region)[3].

The final regime, annular dewetting, is shown in Figure 3C (for the case of 82.0 mM SDS and H = 0.45 mm). This regime evolves similarly to the annular depression regime. The dome is still present in the region of deposition, but now the annular region surounding it becomes completely devoid of liquid. While Figure 3C shows an apparently finite height of liquid in the region of dewetting, this is actually dye which has been deposited on the surface during the spreading event. If it is assumed the dye maintains the same extinction coefficient in this deposited state, the apparent film thickness calculated from the optical density in the dewet region would correspond to approximately roughly a “monolayer” of deposited dye (supplimental information Section S.1. (Other direct evidence for dewetting in this annular region is discussed below.) The Marangoni ridge moves outward in front of this dewet region and continues to do so even after the annulus is fully dewet. The dewet region widens as time advances until reaching a limiting size.

While most of this study examines behaviors that occur before the Marangoni front interacts with the petri dish wall, important data were also collected on how long it took the films to return to their original thickness after the Marangoni spreading event. For experiments in the central depression regime, the flat surface reforms in ~2 s, as soon as the reflections of the

ridge dissipate. In the annular depression regime, the thinned region can persist significantly longer than the reflections of the Marangoni ridge (2–60 s) with smaller G values leading to longer healing times. This suggests a hydrodynamic inhibition to flow back to the central dome on time scales even larger than the initial spreading event. Finally, the annular film rupture that occurs in the dewetting regime is “permanent”; the film never heals when observed for times as long as a day until the ruptured film evaporates. Whereas at the beginning of the experiment, the dye solution subphase wets the glass dish, after the spreading event in the annular dewetting regime, the liquid is pinned at either edge of the dewet region. This contact line pinning suggests that the dye and/or surfactant are depositing from the solutions in the subphase and/or drop onto the glass in the dewet region and locally modifying the surface energy of the dish. Accordingly, when drops of pure water or of a surfactant solution with the same concentration as that used to initiate spreading are placed on the dewet region, the drops bead up with a significantly larger contact angle than on the initial clean glass surface.

An operating diagram constructed in Figure 4 identifies the conditions under which each hydrodynamic regime occurs. Lines of constant gravitational parameter G were calculated using the measured surface tension corresponding to each initial SDS solution concentration in the drop (accounting for the dye concentration) and superimposed on the operating diagram. Prior modeling demonstrated that the magnitude of the G parameter captures important trends with respect to the onset time and strength of recirculation flows that dominate the film height profile. The scaling of G with H^2/S implies a significant sensitivity to subphase depth and surfactant concentration[3]. For $G > 1$, recirculation flows occur with the onset of spreading. At large SDS concentrations, transitions from annular dewetting to annular depression and then to central depression regimes occur near $G = 0.1$ and $G = 1.0$, respectively. Extending the lines of constant G to lower SDS concentrations shows that the transitions are not simply predicted by the value of G: Measured transitions from annular depression to central depression do not map onto the lines of constant G for lower SDS concentrations, although the annular dewetting to annular depression tranistion is still well approximated by a constant $G = 0.1$ line. In general, the central depression regime is favored by low surfactant concentrations or large subphase film depths. Annular dewetting is limited to smaller film depths but can occur both above and below the CMC.

At very large surfactant concentrations, the experimental data collected in this study agrees with the theoretical predictions. Recirculation flows occurring in the central depression regime only appear at $G > 1$ in the models. This is consistent with the central depression regime occurring just above $G = 1$ at high SDS concentrations. Additionally, the onset of the annular dewetting regime also appears to be affected by the G parameter, occuring when $G < 0.1$ for high SDS concentrations. However, as sufactant concentration is reduced, the central depression regime appears at values where the G parameter would predict no recirculation at the onset of spreading. This is a result of the depletion effect described by Lee and coworkers[27]. While the surface tension of all drops containing 6 mM or greater SDS concentration (the CMC in the presence of the dye) would have the same initial surface tension difference relative to the clean subphase, the surface tension difference may change during the spreading event due to depletion below a threshold SDS concentration in the region of deposition. The point at which this depletion occurs will be different depending on

the initial surfactant inventory in the drop and is expected to reduce the Marangoni stress imposed across the surface. The initial SDS concentration that identifies the threshold for depletion is marked by a vertical reference line on the operating diagram. The depletion concentration was determined by calculating the number of molecules required to fully pack the surface, then adding to that the number of molecules required in the drop volume to keep the region of initial deposition above the CMC; it was assumed that there was no desorption of surfactant into the underlying film and that the surfactant packing density at the surface was 52.5Å^2/molecule[31]. This depletion of the surfactant from the drop has a large effect on the spreading behavior when compared to the predictions for the nondepleted cases explored in the literature, with recirculation and the associated central depression regime here occuring at far lower G values than expected. Notably, the SDS concentration at which the annular depression to central depression transition begins to deviate from $G = 1.0$ matches the predicted onset of depletion effects. Defining these three regimes and when they occur allows for the characterization of distinct flow and transport behaviors in these regimes.

The operating diagram describes the trends in the hydrodynamic regime boundaries for behavior after a fixed real time, 233 ms. Gaver and Grotberg suggest that different behaviors should occur for different G values at different dimensionless times. However, if the operating diagram were plotted using the non-dimensional time suggested in the analysis of Marangoni spreading on thin films, the trends in the boundaries of the hydrodynamic regimes remain the same. In spreading analyses, time is scaled as $\tilde{t} = \frac{SH_0}{\mu L^2}t$, where μ is the subphase viscosity, L is the length scale of the surface tension gradient, t is the dimensional time (233 ms for this operating diagram), and $\tilde{t}$ is the dimensionless time[26,32].

This brings up an important question, would the location of the transitions between behaviors change if the points were plotted at the same dimensionless time? The major feature of the operating diagram, the sharp decrease in the transtion between the central depression and annular depression regimes would appear much the same. Each horizontal line of points above the CMC is already at the same dimensionless time since H_0 and S are the same. Also, the change in G associated with changing H_0 on the verticle lines of points shows the same behavior as is shown on figure one when the points are adjusted to the same dimensionless time. While the exact position of the operating boundary may shift slightly, the qualitative effects of depletion significantly effecting the location of the transition are the same.

3.3 Features of the Marangoni Spreading that Impact Transport Processes

Because of their relevance to transport rates of solvent or solutes advected in the Marangoni spreading flow, two features of the Marangoni ridge were tracked: the net outflow volume and the Marangoni ridge velocity. Figure 5 shows the the net outflow volume for each of the liquid depths and surfactant concentrations studied, calculated at the last time step before the Marangoni ridge reaches the edge of the dish (233 ms). As shown in the inset of Figure 5, net outflow volume is defined as the total volume of liquid displaced by the movement of the Marangoni ridge, relative to the initial flat surface condition. This volume is dictated by the competition between the outward Marangoni flow and any counteracting recirculation flow.

First, consider the effect of surfactant concentration. For any film depth considered here, the outflow volume increases with increasing surfactant concentration. This is true for solutions below the CMC (1.0 and 4.1 mM SDS) where increasing concentration decreases surface tension and thereby increases the initial Marangoni driving force. It is also true for solutions above the CMC (20.5 and 82.0 mM SDS), where for any considered film depth, outflow volume increases with increasing SDS concentration above the CMC despite the fact that the initial surface tension remains constant. The decreased outflow volume for the less concentrated of two micellar solutions (20.5 mM), having by default the same initial surface tension as the more concentrated micellar solution (82.0 mM), implicates depletion of the surfactant during the spreading event as the cause. The less concentrated micellar solution has a concentration near the predicted threshold for depletion (Figure 4) and is therefore unable to sustain the outward Marangoni flow, unlike the more concentrated micellar solution.

Initial film depth also strongly influences the outflow volume. For a fixed surfactant concentration, the outflow initially increases with increasing film depth, eventually reaching a plateau or passing through a maximum. For low SDS concentrations, the outflow volume does pass through a maximum with increasing film depth. This may be because recirculation flows play a more prominent role in thicker films (larger G), and recirculation counteracts outflow. The closely related consequence of increasing H at constant S (increasing G), is that it may drive the system from one hydrodynamic regime to another. Note that the highest SDS concentration data, 82.0 mM, shows the most pronounced maximum and has significantly lower net outflow volume in the central depression regime than in the annular depression regime.

The dependencies of Marangoni ridge velocity on initial film depth and surfactant concentration are shown in Figure 6. The ridge velocity is calculated by tracking the position of the maximum of the Marangoni ridge with time for several (n=3) trials. While the data are compatible with power laws with powers in the ranges predicted for the Marangoni ridge movement [33], the powers cannot be reliably obtained from the data because of the limited time range of the data, the limited number of data points, and the strong correlation between the variables in the power law fit. If we use a simple average ridge velocity over the time interval of the experiment, that average velocity increases with increasing surfactant concentration for a given initial film depth. The dependence of the ridge velocity on initial film depth is weak, except for film depths below approximately 0.5 mm. At these depths, the Marangoni ridge velocity is significantly decreased. Notably, at these depths, the height of the Marangoni ridge (approximately 0.2 mm) is comparable to the initial film depth.

There is a stark contrast in the film depth dependence for outflow volume and Marangoni ridge velocity. Examining the trends shows that outflow volume behaviors change significantly with changing hydrodynamic regime, whereas the Marangoni ridge velocity does not. The main difference between the hydrodynamic regimes is the complex change in the recirculation flows in the bulk of the film. The results suggest that the outflow volume is more strongly influenced by the bulk flow including recirculation, whereas the ridge velocity, a direct result of the stress condition at the interface and the more localized flow

associated with the ridge, is not as strongly influenced by bulk flow effects except for the thinnest films.

3.4 Fate of the Drop Contents

Solute-tracking experiments with dye included only in the drop made it possible to determine the extent to which transport of drop contents during the spreading event may exhibit distinct behaviors with respect to the hydrodynamic regime. Figure 7 shows typical optical density profiles recorded as spreading proceeded during one such experiment in the central depression regime. For all of the experiments, regardless of hydrodynamic regime, the profile consists of two portions: the high optical density region at the center of the region of deposition representing the main portion of the drop as it coalesces with the subphase and the lower, but more extended optical density region representing “escape” of the dye from the drop. The escaped dye region broadens more extensively with time than does the drop region. Note that the dye concentration in the drop was chosen to be much higher than that used in the surface profile experiments above in order to obtain better information on solute presence in the escape region. However, this resulted in measured optical density values in the drop region that were beyond the linear range of the Beer-Lambert Law; the amount of dye in the drop region cannot be accurately calculated. Validation experiments with lower dye concentrations in the drop show conservation of the dye during the spreading event to within 5% but are unable to detect escaped dye.

Profiles from all three hydrodynamic regimes exhibit both a drop region and an escape region described above, but they differ significantly in the relative amounts of dye in the escaped dye region, as shown in Figure 8. This figure focuses on the column densities of dye (number of dye molecules per unit projected area) in the escaped dye region. As with the other experiments, results are only shown for video frames up to the last frame before the Marangoni ridge reached the petri dish wall in order to minimize extrinsic effects on spreading phenomena. The edges of the drop region can be discerned in Figure 8 as the steep portion of the curves closer to the origin. This drop edge moves outward with time. Outside the drop edge, a region of nearly constant column density appears, with an abrupt decrease to baseline further out. This feature is well defined in the central depression and annular depression regimes. The radial length of this constant column density region grows far beyond the edge of the drop. In the central depression regime and annular depression regime, the escaped dye transports at similar rates. Furthermore, the dye is transported significantly further in those regimes than in the annular dewetting regime. The maximum columnar dye density is also significantly greater in the central depression and annular depression regimes than in the annular dewetting regime.

In the annular depression regimes, at longer times, most of the dye is observed to be contained in the drop region until the thinned region is healed (which requires ~60 s, well beyond the time range of Figure 8). In the annular dewetting regime, dye transport in the escaped dye region is greatly reduced. Only a small amount of dye is able to escape the central drop region before the thin annulus ruptures and dewets. The dewetting region then traps all remaining dye in the now stranded central drop. Fingering instabilities were observed near the inner edge of the dewet region, after this trapping occurred at the edges of

the stranded drop, consistent with those described in the literature for spreading surfactant solutions[24,34,35] (Figure S6). Fingering was only observed in the annular dewetting regime.

Figure 9 shows the extent to which the edge of the drop region had migrated outward by 233 ms, just before the ridge meets the petri dish wall. The drop edge is defined as the point where the optical density shows a sharp decrease in slope as it meets the escaped dye region, as sketched in the Figure 9 inset. For all conditions examined, the spreading of this drop region is similar regardless of the subphase depth, surfactant concentration or hydrodynamic regime. Therefore, even though a surface tension gradient drives spreading beyond the drop, surface tension gradients and Marangoni stresses have no significant effect on spreading of the drop itself, which is likely dominated by gravity and surface tension.

The radial extent of dye spreading the escaped dye region depends on the hydrodynamic regime. In the central and annular depression regimes, the extent of escaped dye spreading is similar, but the extent of spreading is reduced as the system moves further into the annular dewetting regime (Figure 10). This is caused by the dewet region cutting off flow between the dye-rich drop region and the rest of the subphase and the slowing of the Marangoni ridge at very thin initial depths. However, despite the significantly different hydrodynamic behaviors in the central and annular depression regimes (specifically the occurrence of recirculation), those regimes yield similar radial extents of dye spreading. This indicates that dye transport is most likely occurring in a thin layer near the surface, where it is not greatly affected by the recirculation flows of the central depression regimes. For the control experiment conducted without surfactant, no dye escaped the drop region.

In applications of Marangoni driven spreading such as pulmonary drug delivery, both the amount of transported solute (drug in that application) and the distance over which it is transported outside the deposition site are critical. Figure 11 presents the mass of dye that escape s the drop, calculated by integrating the columnar density over the escaped dye region area as illustrated in the inset. The total mass of dye transported as “escaped dye” beyond the drop edge increases while the system transitions from the annular dewetting to the annular depression to the central depression regimes. The amount of dye transported in the central depression region is similar to, and for 8 mM SDS, somewhat larger than, the amount in the annular depression regime, despite the fact that recirculation occurs throughout the central depression spreading event. One particularly interesting result observed for larger film thicknesses is that more dye is transported with lower concentrations of surfactant, as this shifts the behavior further toward the central depression regime. Comparing the transport of dye to the net outflow of the subphase (Figure 5), the two do not have the same trends. While increasing surfactant concentration increases net fluid outflow, decreasing the concentration (and moving the system towards the central depression regime) leads to increased dye transport. The ability to control these two phenomena independently, may be important when designing for processes where material transport from the drop is desired while subphase transport is not, as is the case in pulmonary drug delivery.

Figure 12 shows results from the subphase height profile experiments and the separate dye-tracking experiments at various time points during spreading. These experiments were

conducted separately, but the comparison of average results obtained from each type of experiment when conducted under the same conditions of subphase depth and surfactant concentration yields useful insights. While the dye content of the spreading solutions was different between the two types of experiments at 82.0 mM where all the data in Figure 12 was taken, initial drop surface tension was the same and depletion should not occur. The dye front is defined as the leading edge of the “escaped dye” region in the dye-tracking experiments. The Marangoni ridge is the position of the maximum height. Regardless of hydrodynamic regime, for any given instant of time during spreading, the dye front coincides with the Marangoni ridge. The data may suggest that the dye front advances slightly ahead of the ridge, but in this case where the dye tracking and Marangoni ridge experiments come from separately executed experiments, it may be unwise to draw too fine a distinction on this matter. As noted above, the mechanistic origin of the Marangoni ridge is the sharp transition in the tangential stress boundary condition, which indicates that the leading edge of surfactant should be in the vicinity of the Marangoni ridge. Using a fluorescent surfactant, Fallest and coworkers concluded that surfactant moves with the peak of the Marangoni ridge[29]. The current results indicate that not only does surfactant migrate far from the drop edge, but that the drop contents keep pace with the migrating surfactant. This solute originating in the drop is transported over distances many times larger than the drop size, although the total amount of solute transported by this means is a small fraction of the total amount of solute in the drop.

3.4 Transport on Complex Subphases

Some applications where this type of Marangoni spreading may be important involve subphases more complex than pure water. For example, in the lungs spreading may occur on films of mucus which are significantly more viscous than water and may be non-Newtonian. Industrial coating flows typically involve concentrated macromolecular solutions or suspensions. To begin to address the issue of subphase complexity, a series of spreading experiments were conducted on 1 wt% aqueous, entangled polyacrylamide (5 – 6 MDa) solutions. This subphase has a surface tension of 70.8 ± 0.5 mN/m, close to that of the aqueous dye solutions considered above and therefore indicating very little polyacrylamide adsorption to the surface. The solutions have a density of 1.00035 ± 0.00005 g/mL, nearly identical to that of water, and a viscosity of ~45 mPa s, about 45 times that of water[36]. Qualitative spreading behaviors were quite similar to those on water, although the spreading events were significantly slower: 2–3 s was typically required for the Marangoni ridge to reach the petri dish wall as opposed to 233 ms for the simple aqueous subphase. All experiments were performed with 82.0 mM SDS, and heights were varied within the same range considered with the simple water subphase.

The primary quantitative difference was that the transitions between hydrodynamic regimes were all shifted to significantly larger film thicknesses compared to the simple subphase. (See Supplemental Information Figure S7). This behavior occurs, even when considering the same dimensionless times during spreading (45 times longer on the polyacrylamide, due to its 45 fold increase in viscosity). The transition between annular depression and annular dewetting occurs from 0.6 mm to 1.2 mm for experiments done at 82.0 mM SDS concentration with the complex subphase (corresponding to a four-fold increase in G at the

transition). No transition between the annular and central depression regimes was observed for subphase film thicknesses up to 2.4 mm, the largest thickness considered for the simple aqueous subphases. There are three possible causes for this change. First, viscosity may have a larger impact on flow behavior than was anticipated in the scaling of the problem[32]. Secondly, the surface equation of state for SDS on polyacrylamide may be different than the corresponding equation on water, leading to different dynamic spreading behavior. Lastly, the problem formulation with a drop of one viscosity deposited on a fluid with a much higher viscosity may pose additional complications arising from the differing viscosities[26].

4. Conclusions

Building on previously reported theoretical [3,15,28,37] and experimental[29,38] studies of Marangoni flow from a localized surfactant deposition, this work used a novel technique to quantitatively measure the Marangoni flow and map the conditions at which key flow regime transitions occur. The results revealed the significant effects that previously identified surfactant depletion effects[39] have on the transport behavior and flow regime transitions. Prior literature had not resolved the relationship between the Marangoni flow hydrodynamics and the transport of components of a surfactant solution deposit. The ability of the technique used here to track the Marangoni ridge as well as the leading edge of the drop contents showed that they move radially outward in tandem.

By varying the liquid film thickness and surfactant concentration, three distinct hydrodynamic regimes occur in response to deposition of an aqueous surfactant solution drop on an aqueous subphase. For any surfactant concentration (ranging from 1.0 to 82.0 mM sodium dodecylsulfate, spanning the critical micelle concentration) increasing the subphase depth results in a transition from the annular dewetting regime, to the annular depression regime, to the central depression regime. Below some low thickness threshold (0.45 mm in the current study), only annular dewetting behavior is observed, regardless of surfactant concentration. Above some upper threshold thickness (1.8 mm in the current study), only the central depression regime is observed for any surfactant concentration considered. At intermediate subphase depths, decreasing surfactant concentrations may produce transitions from annular depression to central depression or from annular dewetting to annular depression.

Depletion of the surfactant in the region of deposition can lead to changes in the hydrodynamic spreading regime. When depletion does not occur, the transition between central depression and annular depression occurs near a gravitational parameter value of $G = 1$, as predicted by Gaver and Grotberg[3]. However, for lower surfactant concentrations for which depletion occurs during spreading, this transition shifts to lower values of G due to the decreasing surface tension gradient during the spreading event. The transition between annular depression and annular dewetting, although not predicted in the literature, is observed to occur near $G \sim 0.1$ both with and without depletion.

The transport properties of the system are dependent on the hydrodynamic regime. While the front of the dye solute that marks the drop contents always tracks the Marangoni ridge, and the solute always escapes the initial drop deposit region for all conditions, the degree to

which this occurs is affected by regime. In the annular dewetting regime, transport of drop contents is severely limited both in how far material is transported and how much material is transported. Despite the differences in bulk recirculation flow behavior between the annular depression and central depression regimes, the distance over which the escaped dye is transported is similar for the annular and central dewetting regimes, as is the total mass of transported dye. The expansion of the drop region is not dependent on the hydrodynamic regime.

Net fluid outflow from the region of deposition does not directly correlate with dye transport. For a constant film thickness, decreasing surfactant concentration leads to reduced net outflow but increased dye transport and increased Marangoni ridge velocity. This would indicate a difference between phenomena that occur very close to the surface (drop contents transport, Marangoni ridge motion) and phenomena that occur in the bulk of the film (net outflow).

The work on higher viscosity, complex subphase films shows that while qualitative behaviors are the same as those for a simple subphase, the conditions marking transitions between hydrodynamic regimes are significantly different. Since the gravitational parameter alone cannot account for these differences, further research is recommended to examine the effects of viscosity on Marangoni flows in thin films, both experimentally and theoretically, and including cases of viscosity mismatch between the surfactant deposit and the subphase. A computational parametric study varying properties such as fluid depth, fluid viscosity, surfactant equations of state and surfactant adsorption and desorption kinetics would also help to better understand the behaviors of a spreading surfactant drop and supplement the current literature.

Supplementary Material

Refer to Web version on PubMed Central for supplementary material.

Acknowledgements

The authors would like to thank Dr. S. Tristram-Nagle for the use of a light table for the described apparatus. This material is based in part on work supported by the National Science Foundation under Grant CBET-1510293 and in part by the National Heart, Lung and Blood Institute of the National Institutes of Health under grant R01 HL105470. The content is solely the responsibility of the authors and does not necessarily represent the official views of the National Science Foundation or the National Institutes of Health.

References

1. Stetten AZ, Iasella SV, Corcoran TE, Garoff S, Przybycien TM, Tilton RD. Surfactant-induced Marangoni transport of lipids and therapeutics within the lung. Curr Opin Colloid Interface Sci 2018;36:58–69. 10.1016/j.cocis.2018.01.001. [PubMed: 30147429]
2. Iasella SV, Stetten AZ, Corcoran TE, Garoff S, Przybycien TM, Tilton RD. Aerosolizing Lipid Dispersions Enables Antibiotic Transport Across Mimics of the Lung Airway Surface Even in the Presence of Pre-existing Lipid Monolayers. J Aerosol Med Pulm Drug Deliv 2017;31:212–20. 10.1089/jamp.2017.1412. [PubMed: 29053080]
3. Gaver DP, Grotberg JB. Droplet spreading on a thin viscous film. J Fluid Mech 1992;235:399–414.
4. Gaver DP, Grotberg JB. The dynamics of a localized surfactant on a thin film. J Fluid Mech 1990;213:127–47. 10.1017/S0022112090002257.

5. Zhang YL, Matar OK, Craster RV. A theoretical study of chemical delivery within the lung using exogenous surfactant. Med Eng Phys 2003;25:115–32. 10.1016/S13504533(02)00190-X. [PubMed: 12538066]
6. Theodorakis PE, Müller E a., Craster RV, Matar OK. Insights into surfactant-assisted superspreading. Curr Opin Colloid Interface Sci 2014;19:283–9. 10.1016/j.cocis.2014.04.007.
7. Khanal A, Sharma R, Corcoran TE, Garoff S, Przybycien TM, Tilton RD. Surfactant Driven Post-Deposition Spreading of Aerosols on Complex Aqueous Subphases. 1: High Deposition Flux Representative of Aerosol Delivery to Large Airways. J Aerosol Med Pulm Drug Deliv 2015;28:282–239. 10.1089/jamp.2014.1168.
8. Sharma R, Khanal A, Corcoran TE, Garoff S, Przybycien TM, Tilton RD. Surfactant Driven Post-Deposition Spreading of Aerosols on Complex Aqueous Subphases. 2: Low Deposition Flux Representative of Aerosol Delivery to Small Airways. J Aerosol Med Pulm Drug Deliv 2015;28:394–405. 10.1089/jamp.2014.1167. [PubMed: 25757067]
9. Sexauer WP, Fiel SB. Aerosolized Antibiotics in Cystic Fibrosis. Semin Respir Crit Care Med 2003;24:717–26. 10.1055/s-2004-815667. [PubMed: 16088587]
10. Corcoran TE, Thomas KM, Garoff S, Tilton RD, Przybycien TM, Pilewski JM. Imaging the Postdeposition Dispersion of an Inhaled Surfactant Aerosol. J Aerosol Med Pulm Drug Deliv 2012;25:290–6. 10.1089/jamp.2011.0920. [PubMed: 22393908]
11. Hattrup CL, Gendler SJ. Structure and function of the cell surface (tethered) mucins. Annu Rev Physiol 2008;70:431–57. 10.1146/annurev.physiol.70.113006.100659. [PubMed: 17850209]
12. Evans PL, Schwartz LW, Roy RV. A Mathematical Model for Crater Defect Formation in a Drying Paint Layer 2000;205:191–205. 10.1006/jcis.2000.6877.
13. Gupta D, Sarker B, Thadikaran K, John V, Maldarelli C, John G. Sacrificial amphiphiles: Eco-friendly chemical herders as oil spill mitigation chemicals. Sci Adv 2015;1:1–6. 10.1126/sciadv.1400265.
14. Stetten a. Z, Moraca G, Corcoran TE, Tristram-Nagle S, Garoff S, Przybycien TM, et al. Enabling Marangoni flow at air-liquid interfaces through deposition of aerosolized lipid dispersions. J Colloid Interface Sci 2016;484:270–8. 10.1016/j.jcis.2016.08.076. [PubMed: 27623189]
15. Afsar-Siddiqui AB, Luckham PF, Matar OK. The spreading of surfactant solutions on thin liquid films. Adv Colloid Interface Sci 2003;106:183–236. 10.1016/S00018686(03)00111-8. [PubMed: 14672848]
16. Matar OK, Craster RV. Dynamics of surfactant-assisted spreading. Soft Matter 2009;5:3801 10.1039/b908719m.
17. Berg JC. An Introduction to Interfaces & Colloids: The Bridge to Nanoscience. Singapore: World Scientific Publishing; 2010.
18. Sharma R, Corcoran TE, Garoff S, Przybycien TM, Swanson ER, Tilton RD. Quasi-immiscible spreading of aqueous surfactant solutions on entangled aqueous polymer solution subphases. ACS Appl Mater Interfaces 2013;5:5542–9. 10.1021/am400762q. [PubMed: 23705869]
19. Trefethen LM, Churchil J. Surface tension in fluid mechanics. Educational Services, Inc.; 1969.
20. Bull JL, Nelson LK, Walsh JT, Glucksberg MR, Schurch S, Grotberg JB. Surfactant-Spreading and Surface-Compression Disturbance on a Thin Viscous Film. J Biomech Eng 1999;121:89–98. 10.1115/1.2798049. [PubMed: 10080094]
21. Jensen OE, Grotberg JB. Insoluble surfactant spreading on a thin viscous film: shock evolution and film rupture. J Fluid Mech 1992;240:259–88. 10.1017/S0022112092000090.
22. Zhang YL, Craster RV, Matar OK. Surfactant driven flows overlying a hydrophobic epithelium: Film rupture in the presence of slip. J Colloid Interface Sci 2003;264:160–75. 10.1016/S0021-9797(03)00449-1. [PubMed: 12885532]
23. Grotberg JB, Gaver DP. A Synopsis of Surfactant Spreading Research. J Colloid Interface Sci 1996;178:377–8.
24. Warner MRE, Craster RV, Matar OK. Fingering phenomena associated with insoluble surfactant spreading on thin liquid films. J Fluid Mech 2004;510:169–200. 10.1017/S0022112004009437.
25. Craster RV, Matar OK. Numerical simulations of fingering instabilities in surfactant-driven thin films. Phys Fluids 2006;18:32103–1–12. 10.1063/1.2180776.

26. Karapetsas G, Craster RV, Matar OK. Surfactant-driven dynamics of liquid lenses. Phys Fluids 2011;23:122106–1–122106–16. 10.1063/1.3670009.
27. Lee KS, Starov VM. Spreading of surfactant solutions over thin aqueous layers at low concentrations: Influence of solubility. J Colloid Interface Sci 2009;329:361–5. 10.1016/j.jcis.2008.10.031. [PubMed: 18973905]
28. Matar OK, Craster RV. Dynamics of surfactant-assisted spreading. Soft Matter 2009;5:3801 10.1039/b908719m.
29. Fallest DW, Lichtenberger AM, Fox CJ, Daniels KE. Fluorescent visualization of a spreading surfactant. New J Phys 2010;12:073029,1–12. 10.1088/1367-2630/12/7/073029.
30. Afsar-Siddiqui AB, Luckham PF, Matar OK. Unstable spreading of aqueous anionic surfactant solutions on liquid films. Part 1. Sparingly soluble surfactant. Langmuir 2003;19:696–702. 10.1021/la0258502.
31. Dahanayake M, Cohen AW, Rosen MJ. Relationship of structure to properties of surfactants. 13. Surface and thermodynamic properties of some oxyethylenated sulfates and sulfonates. J Phys Chem 1986;90:2413–8. 10.1021/j100402a032.
32. Gaver DP, Grotberg JB. The dynamics of a localized surfactant on a thin film. J Fluid Mech 1990;213:127–47. 10.1017/S0022112090002257.
33. Jensen OE. The Spreading of Insoluble Surfactant at the Free Surface of a Deep Fluid Layer. J Fluid Mech 1995;293:349–78. 10.1017/S0022112095001741.
34. Warner MRE, Craster RV, Matar OK. Fingering phenomena created by a soluble surfactant deposition on a thin liquid film. Phys Fluids 2004;16:2933–51. 10.1063/1.1763408.
35. Hamraoui A, Cachile M, Poulard C, Cazabat AM. Fingering phenomena during spreading of surfactant solutions. Colloids Surfaces A Physicochem Eng Asp 2004;250:215–21. 10.1016/j.colsurfa.2003.12.035.
36. Stetten AZ, Treece BW, Corcoran TE, Garoff S, Przybycien TM, Tilton RD. Evolution and disappearance of solvent drops on miscible polymer subphases. Colloids Surfaces A Physicochem Eng Asp 2018;546:266–75. 10.1016/j.colsurfa.2018.03.003.
37. Karapetsas G, Craster RV, Matar OK. Surfactant-driven dynamics of liquid lenses. Phys Fluids 2011;23:122106–1–122106–16. 10.1063/1.3670009.
38. Afsar-Siddiqui AB, Luckham PF, Matar OK. Dewetting behavior of aqueous cationic surfactant solutions on liquid films. Langmuir 2004;20:7575–82. 10.1021/la040041z. [PubMed: 15323504]
39. Lee KS, Ivanova N, Starov VM, Hilal N, Dutschk V. Kinetics of wetting and spreading by aqueous surfactant solutions. Adv Colloid Interface Sci 2008;144:54–65. 10.1016/j.cis.2008.08.005. [PubMed: 18834966]

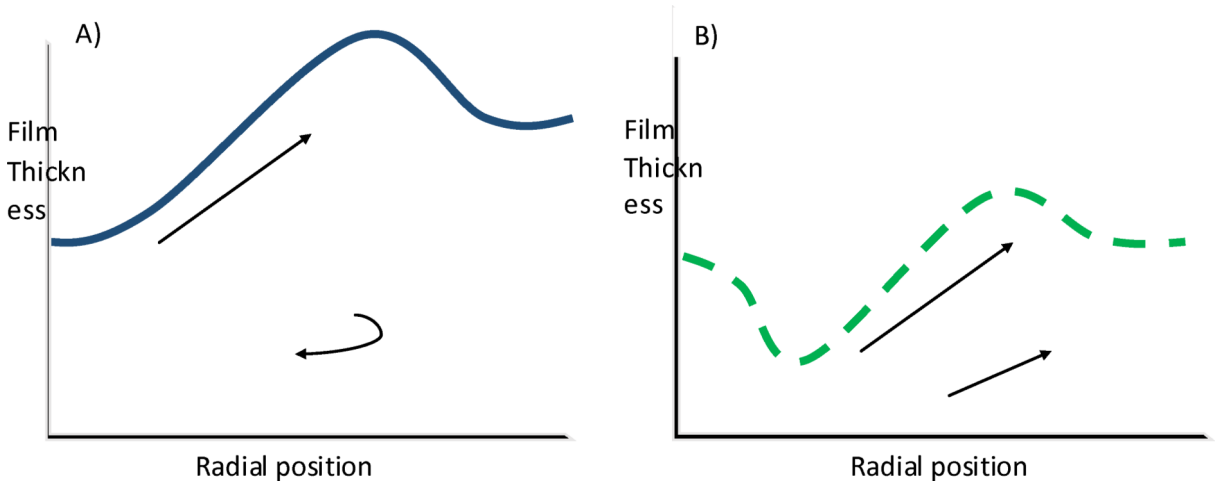

Figure 1.

A simplified schematic of the two spreading behaviors identified by Gaver and Grotberg when recirculation is present (A) and when it is not (B). In both cases, surfactant was initially present in a disk on the undisturbed surface centered at radial position zero[3].

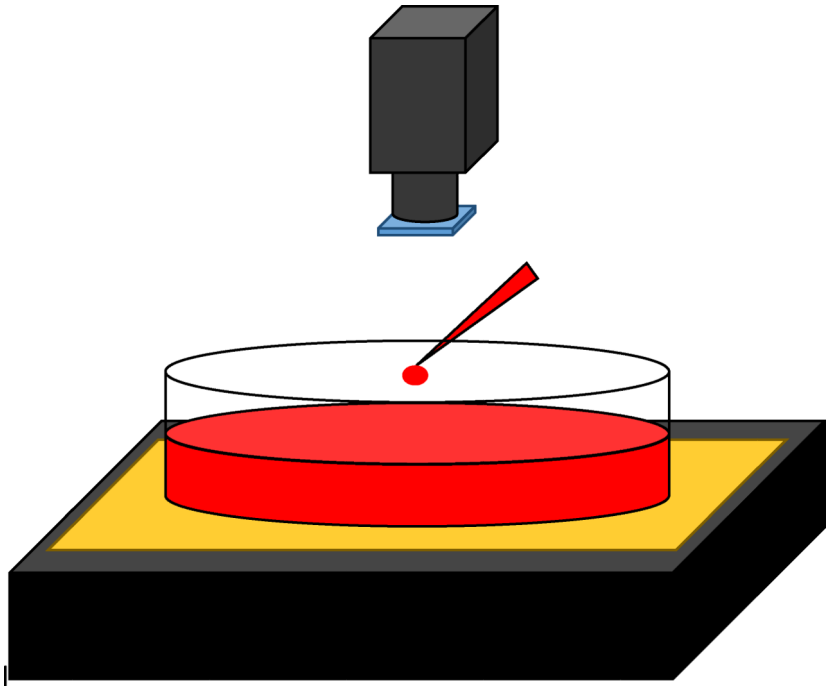

Figure 2.

Experimental setup to measure time dependent subphase height profiles. A 7 cm radius glass petri dish was placed on a light table and filled with a dye-containing liquid film. A single 5 μL drop containing surfactant and dye was deposited on the surface and the spreading event was imaged through a bandpass filter with a digital camera.

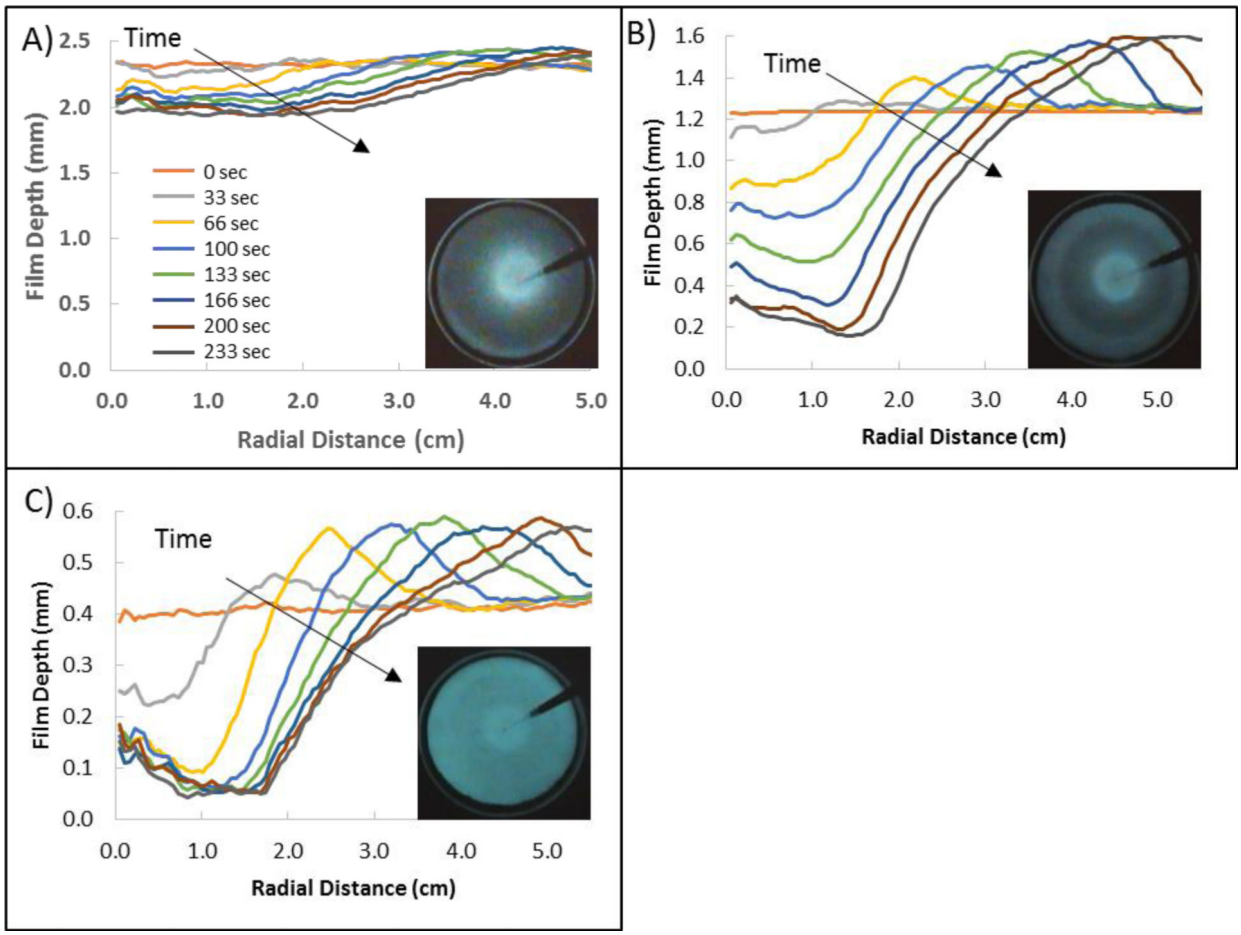

Figure 3.

Azimuthally averaged subphase liquid height profiles during the first 233 ms of spreading in the three hydrodynamic regimes that occur for Marangoni transport. A) Central depression regime, B) annular depression regime, C) annular dewetting regime. Insets show images of transmitted intensity representative of each regime.

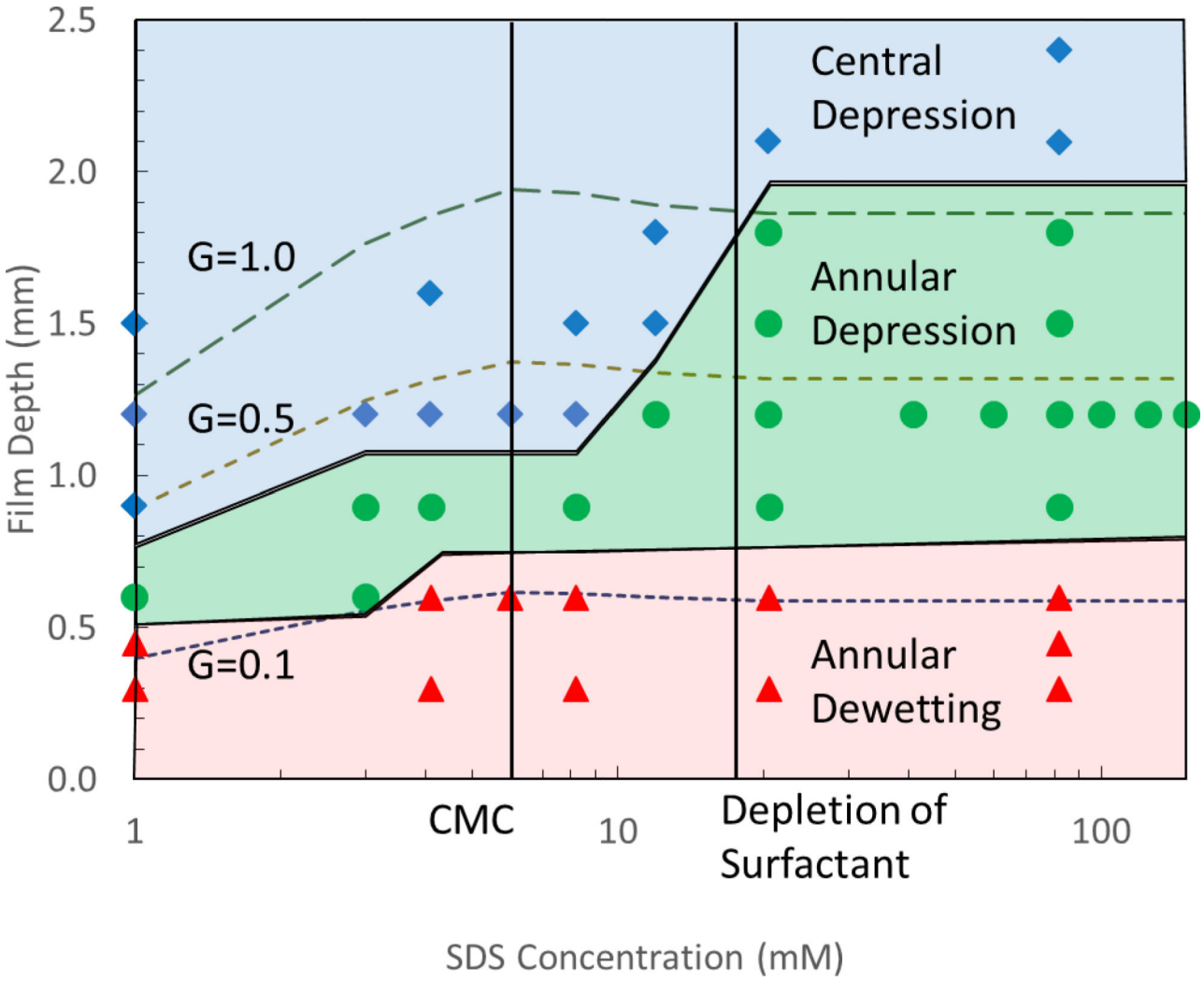

Figure 4.

Operating diagram showing locations of the three hydrodynamic regimes in the film depth/SDS concentration phase space. Triangle, circle and diamond symbols indicate experimental conditions resulting in annular dewetting, annular depression and central depression behaviors, respectively. Dashed curves denote constant gravitational parameter (G) values of 0.1, 0.5, and 1.0. The CMC and the SDS concentration below which surfactant depletion is anticipated to cause the surface tension of the drop to increase during spreading are noted by vertical lines.

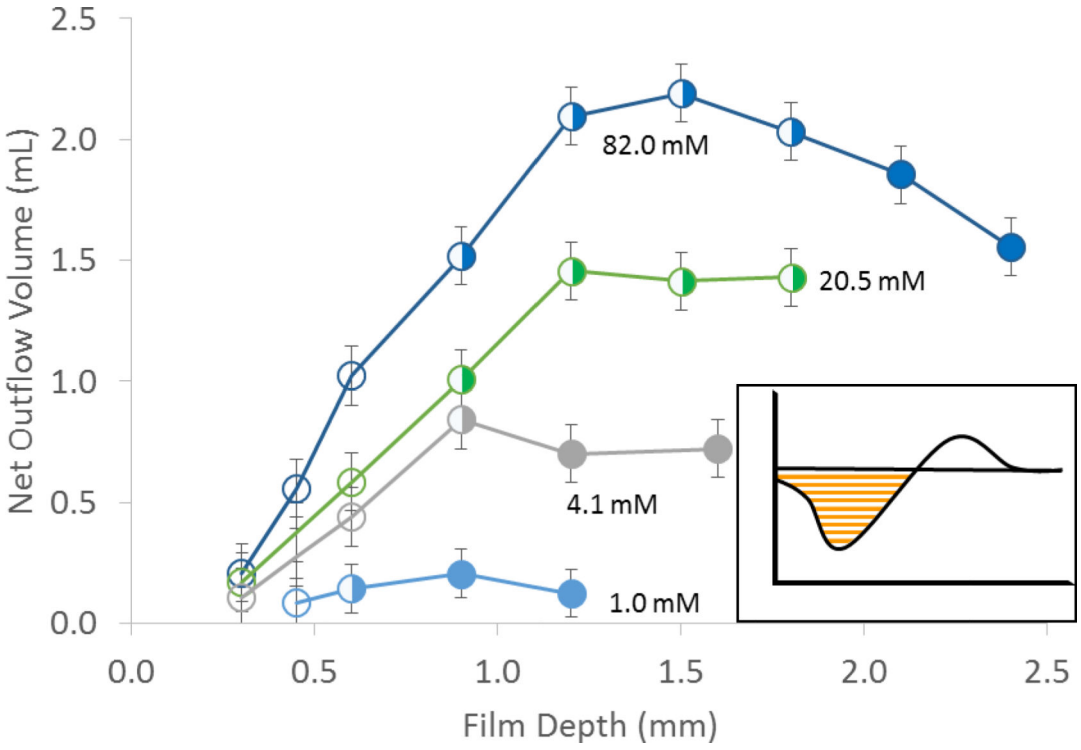

Figure 5.

Net outflow volume at 233 ms for various film depths and SDS concentrations. The inset illustrates the net outflow volume calculation as the radial integration of the volume between the initial (flat) surface height profile and the current height profile to the point of intersection. Solid data points are in the central depression regime, half-filled points are in the annular depression regime, and empty points are in the dewetting regime. Each set of data points is labeled according to the SDS concentration in the deposited drop. Error bars are standard error for n=3 experiments.

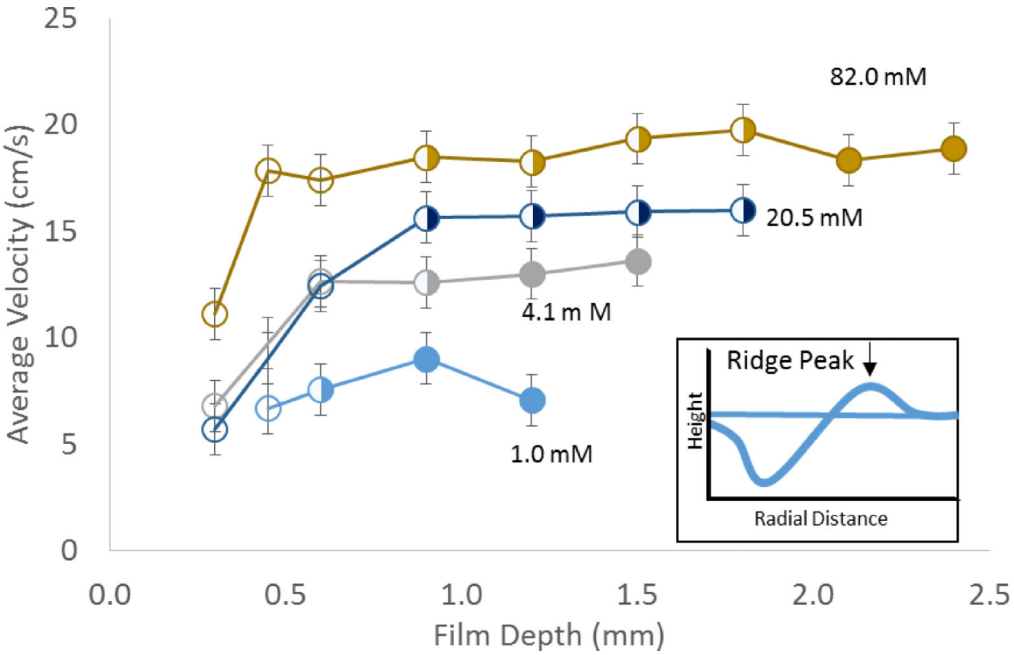

Figure 6.

The average Marangoni ridge velocity for various film depths and SDS concentrations. The inset illustrates the position of the Marangoni ridge used to calculate the Marangoni ridge velocity. Solid points are in the central depression regime, half-filled points are in the annular depression regime, and empty points are in the dewetting regime. Error bars are standard error for n=3 experiments.

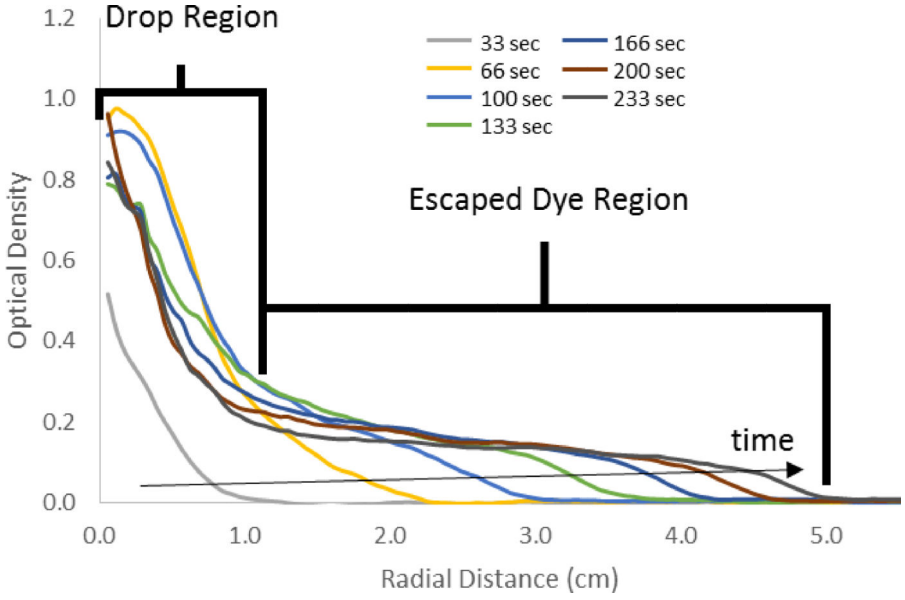

Figure 7.

Azimuthally averaged optical density distributions plotted for discrete times between 0 and 233 ms for a dye-containing drop experiment. The profiles consist of two regions, the inner drop region and the outer escaped dye region. The two regions can be differentiated by a change in slope. The escaped dye region moves out radially with time. Optical densities above 0.6 are outside of the working range of the Beer-Lambert law relation used to calculate amount of dye. These profiles were taken from an experiment in the central depression regime (at 8.5 mM SDS and H = 1.5 mm).

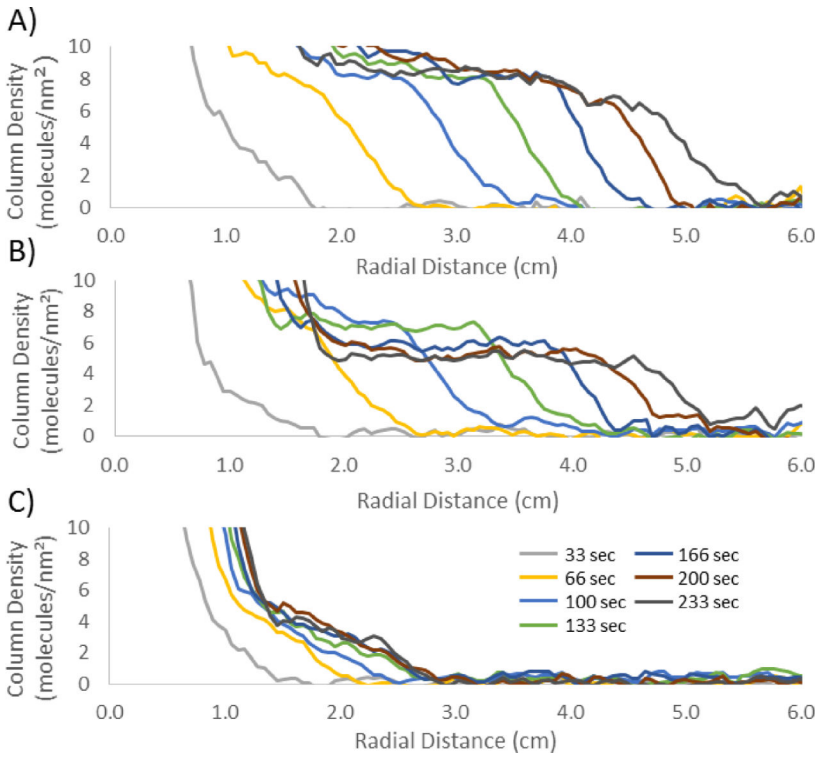

Figure 8.

Dye profiles from 0 to 233 ms for each of the three hydrodynamic regimes. Profiles have been truncated to show the escaped dye region where the dye is transported the farthest. In the central and annular depression regimes, the dye is transported over fairly similar distances, ~ 6 cm, despite the qualitative differences in the hydrodynamic behavior of the bulk film. Dye transport in the escaped region is greatly reduced in the annular dewetting regime, never exceeding ~3.5 cm where the data meets the baseline. This limit increases as the system parameters cause the system to approach the annular depression regime. Data shown is for a SDS concentration of 8.2 mM and film depths of A) 1.5 mm (central depression), B) 0.9 mm (annular depression), and C) 0.3 mm (annular dewetting).

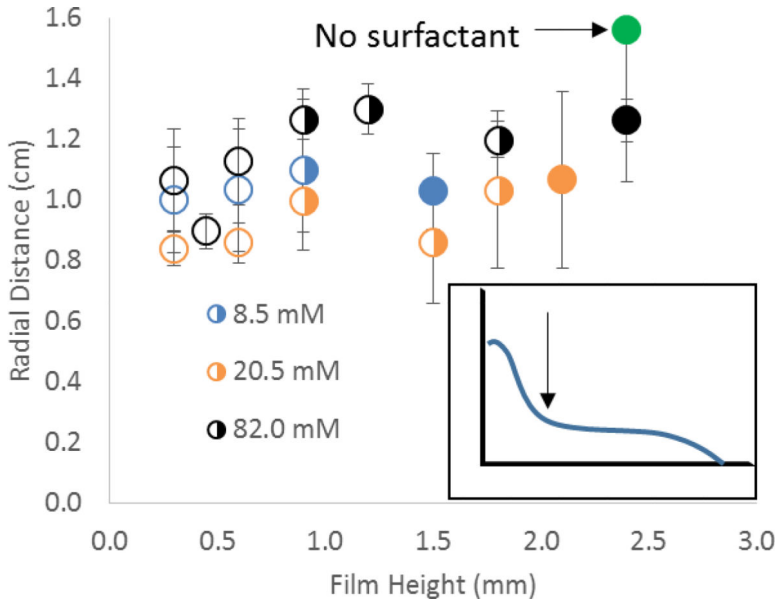

Figure 9.

Position of the drop edge at 233 seconds for various subphase depths and SDS concentrations. Solid points are in the central depression regime, half-filled points are in the annular depression regime, and empty points are in the dewetting regime. Neither concentration, subphase depth, nor hydrodynamic regime has a significant effect on the location of this feature. Error bars are standard error for n=3 experiments.

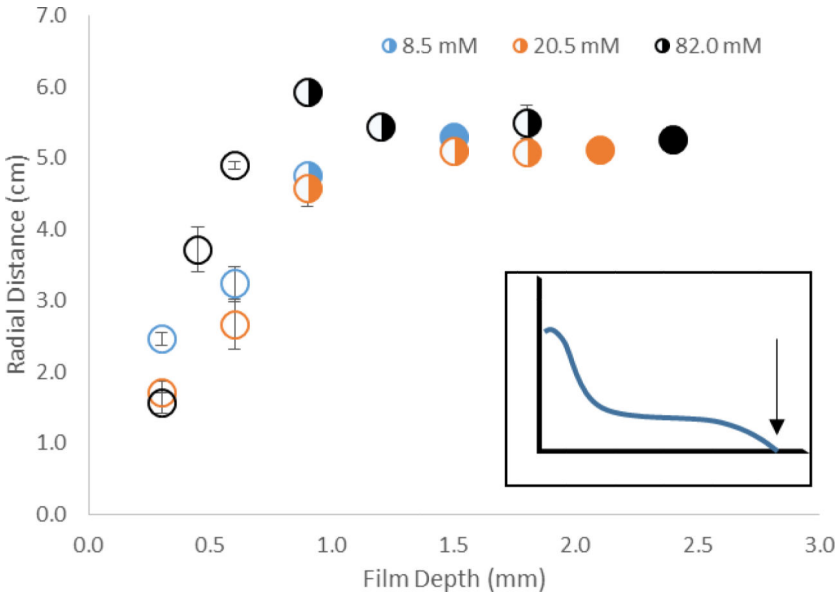

Figure 10.

The radial extent of dye spreading at 233 seconds, for various subphase depths and surfactant concentrations. Solid points are in the central depression regime, half-filled points are in the annular depression regime, and empty points are in the dewetting regime. Error bars are standard error for n=3 experiments.

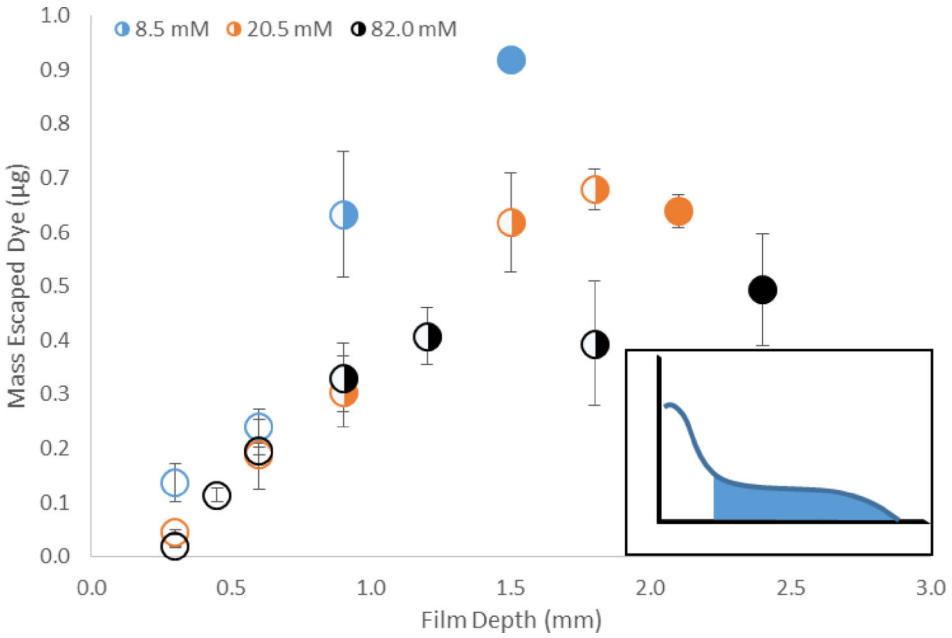

Figure 11.

The mass of escaped dye at 233 ms for various subphase depths and surfactant concentrations. Solid points are in the central depression regime, half-filled points are in the annular depression regime, and empty points are in the dewetting regime. A total mass of 2.5 mg of dye was included in each drop. Error bars are standard error for n=3 experiments.

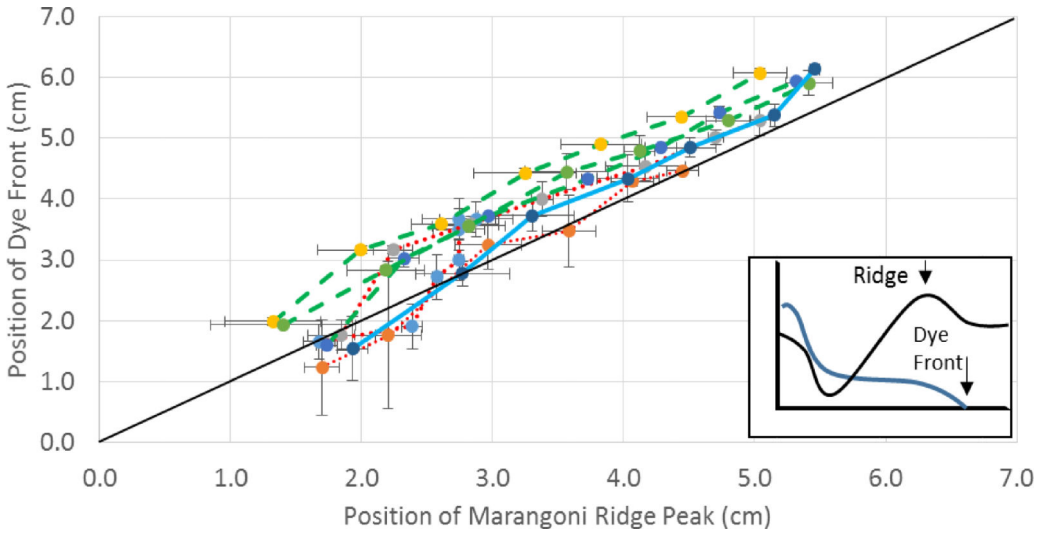

Figure 12.

The position of the dye front compared to the position of the Marangoni ridge peak across different times for each of the three regimes. Solid lines represent the central depression regime, dashed green lines are in the annular depression regime, and dotted red lines are in the annular dewetting regime. Regardless of regime, the dye front tracks the behavior the Marangoni ridge. Each different dot type represents different film height spanning the full range of experimentation. All experiments were done with a surfactant concentration of 82.0 mM. Error bars are standard error for n=3 experiments.